Influence of fluorescence lifetime selections and conformational flexibility on brightness of FusionRed variants

Srijit Mukherjee,[1, 2, 3] Nancy Douglas,[2] and Ralph Jimenez[1, 2]

[1] JILA, University of Colorado, Boulder and National Institute of Standards and Technology, 440 UCB, Boulder, Colorado 80309, United States

[2] Department of Chemistry, University of Colorado, Boulder, 215 UCB, Boulder, Colorado 80309, United States

[3] Department of Chemistry, Stanford University, Stanford CA 94305

KEYWORDS

Fluorescent Proteins, FusionRed, Molecular Dynamics, Photophysics

ABSTRACT

Fluorescent Proteins (FPs) for bioimaging are typically developed by screening mutant libraries for clones with improved photophysical properties. This approach has resulted in FPs with high brightness, but the mechanistic origins of the improvements are often unclear. We focused on improving the molecular brightness in the FusionRed family of FPs with fluorescence lifetime selections on targeted libraries, with the aim of reducing non-radiative decay rates. Our new variants show fluorescence quantum yields up to 75% and lifetimes >3.5 ns. We present a comprehensive analysis of these new FPs, including trends in spectral shifts, photophysical data, photostability, and cellular brightness resulting from codon optimization. We also performed all-atom molecular dynamics simulations to investigate the impact of sidechain mutations. The trajectories reveal that individual mutations reduce the flexibility of the chromophore and sidechains, leading to an overall reduction in non-radiative rates.

Main Text:

Fluorescent proteins (FPs) are commonly utilized as imaging probes and biosensors.[1, 2] Despite the numerous advancements in engineering them over the past three decades, many FPs exhibit low brightness compared to synthetic organic fluorophores.[3] As a result, there is continued demand for improved variants, which are generally being developed by combining rational and random mutagenesis with high throughput screening.[4-11] Although this directed evolution approach has achieved notable success, it typically relies on repeated screenings of large mutant libraries and the molecular basis for the outcomes is often unclear, for example are particular mutations synergistic? These limitations may be overcome by integrating protein design principles based on quantitative, predictive, and generalizable concepts for protein function. Insights from crystallographic structures and spectroscopic studies have guided rational design of FP libraries. However, the most frequently used selection methods such as Fluorescence Activated Cell Sorting (FACS) or microwell-based plate screening do not provide the detailed spectroscopic information obtained from in-vitro studies.[12] As a result, selection efforts usually focus only on characterizing the final product. This approach leaves gaps in understanding intermediates from directed evolution of photophysical properties. Higher information content screening methods, for example, based on fluorescence lifetime selections have been introduced to address this limitation. These platforms have been employed to generate FPs with state-of-the-art brightness such as mScarlet, mTurquoise2, and mCherry-XL.[13-15] This approach has been successful because the fluorescence quantum yield for a closely related set of FPs, e.g., within a library, scales approximately linearly with lifetime, so the improved brightness is primarily due to decreased non-radiative decay rates.[16-19]

We recently combined lifetime-based selections with rational mutagenesis to develop brighter FusionRed (FR) variants, notably FR-MQV (FusionRed L175M, M42Q, C159V; ϕ=0.53; τ=2.8 ns), which is the brightest FR variant to date.[20] FR and its progeny are known for their high fidelity cellular localization and low toxicity,[21-23] utility in live-cell imaging, and gene expression studies.[21-24] Furthermore, the fluorescence blinking of FR variants at the single-molecule level has been utilized in super-resolution microscopy.[25-27] In the course of developing FR-MQV, we identified the M42Q mutation, which resulted in a significant increase (by ~27%) in quantum yield and lifetime (by ~20%). The inspiration to site saturate this position in the sequence stemmed from our ultrafast spectroscopy studies on hydrogen bonding of the acylimine end of the chromophore in closely-related FPs.[28] The L175M mutation in FR-MQV, selected through lifetime screening of libraries generated from error-prone mutagenesis, increased brightness in mammalian cells and extended the lifetime (by ~20%).[29] Finally, the C159V mutation was obtained from lifetime screening of site-directed libraries targeting positions C159, M161, V196, and H198 based on the proximity of these residues to the phenol moiety of the RFP chromophore.[15] Despite these advances, no FR variants have been generated with quantum yields or lifetime that compare with mCherry-XL (ϕ=0.70; τ=3.9 ns) or mScarlet variants (ϕ > 0.70; τ=3.9 ns), thus motivating further research into reducing its non-radiative rate.

Our goal in this study was to explore the mutational landscape of FR, in search of variants with long fluorescence lifetimes and high quantum yields that rival mCherry-XL and mScarlet variants. We focused on reducing non-radiative rate using lifetime screening of individual bacterial colonies, sequence-position-targeted photophysical assessments, and all-atom molecular dynamics (MD) simulations. We surveyed the prospects for improvement beyond FR-MQV with brightness and lifetime flow cytometry on a FACS-enriched random mutagenesis library. We then sequentially targeted individual positions to evaluate the effects of substitutions. MD simulations provided insight into how the substitutions influence conformational diversity of the chromophore environment. With this approach, and with only a few steps

on the mutational manifold, we arrive at bright variants with quantum yields from 60% to 75%. A key finding of our study is that individual mutations leading to brighter FR variants consistently result in reduced conformational heterogeneity, corroborated by measured values of reduced non-radiative rate constants.

Mutagenesis: The fluorescence quantum yield of molecules is approximately linearly proportional to the fluorescence lifetime, which in turn is related to the radiative and non-radiative rate constants governing the depopulation of the excited state, as described by the following equation:

$$\phi = k_{rad} \times \tau = \frac{k_{rad}}{k_{rad} + k_{non-rad}}$$

The radiative rate constant for FR-MQV (k_{rad} = 191 μs^{-1}) is comparable to that of bright FPs such as mScarlet3 (k_{rad} = 186 μs^{-1} & $k_{non-rad}$ = 72 μs^{-1}) and mCherry-XL (k_{rad} = 179 μs^{-1} & $k_{non-rad}$ = 76 μs^{-1}), but its non-radiative rate constant ($k_{non-rad}$ = 169 μs^{-1}) was almost two times higher.[13,15] Therefore we evaluated the potential for the discovery of longer-lifetime FR-MQV variants. First, random mutagenesis (i.e. error-prone PCR; EPPCR) was used to generate libraries with approximately 2, 4.5, and 16 mutations per kilobase at the nucleotide level. Libraries expressed in *E. coli* were enriched by FACS and screened for diversity in fluorescence lifetime (see Supplementary Information S1a and S2a for detailed methodology). We consistently observed a wider distribution of fluorescence lifetime around the mean brightness of the parent FR-MQV in these libraries. The highest-error rate EPPCR library exhibited a 1.25-fold higher variation in fluorescence lifetime compared to the lower error-rate libraries (Table S2.1). The diversity of fluorescence lifetime in these libraries points to the existence of FR-MQV variants with longer lifetimes (details in Supplementary Information S2a).

Next, we designed site-directed libraries at locations known to impact the FP photophysics but which were not thoroughly explored in the previous studies (see Figure 1). These small libraries of 20–400 variants were screened on plates to identify longer-lifetime variants. (Detailed in Supplementary Section S1d) Consequently, we performed saturation mutagenesis at position L175, which was previously identified as a position which led to photophysical diversity.[29] We observed that the L175H substitution resulted in a 1.3-fold increase in fluorescence lifetime and a 1.8-fold increase in quantum yield. We designate this variant "FR-H." We also found that amino acids with larger sidechains, such as methionine (M), arginine (R), and histidine (H), extended the lifetime, whereas those with smaller sidechains, such as serine (S), decreased it relative to FR (see Supplementary Information S2.2b). Pursuing further mutagenesis at position 42 for the FR-M and FR-H, the two variants with the longest lifetimes from the L175X library led to the rediscovery of M42Q as the substitution with the longest lifetime and highest quantum yield. Interestingly, FR-H M42Q (denoted "FR-HQ") had lifetime and quantum yield values exceeding FR-MQV ($\phi_{FR\text{-}MQV}$=0.53; $\tau_{FR\text{-}MQV}$ =2.8 ns v. $\phi_{FR\text{-}HQ}$=0.60; $\tau_{FR\text{-}HQ}$ =3.0 ns). Next, we performed saturation mutagenesis at position C159 on the two variants with the highest lifetime, FR-HQ and FR-MQ (details in Table S2.3 and S2.4). Lifetime screening confirmed that FR-HQ and FR-MQV are the brightest variants in these libraries.

Table 1. Sequence information of variants of FR relevant to the study

FP	42	71	159	175	218
FR	M	I	C	L	A
FR-Q	Q	I	C	L	A
FR-H	M	I	C	H	A
FR-M	M	I	C	M	A
FR-MQ	Q	I	C	M	A
FR-MQV	Q	I	V	M	A
FR-MQVV*	Q	V	V	M	A
FR-HQ	Q	I	C	H	A
FR-HQT	Q	I	C	H	T
FR-HQV*	Q	V	C	H	A
FR-HQTT*	Q	T	C	H	T

`

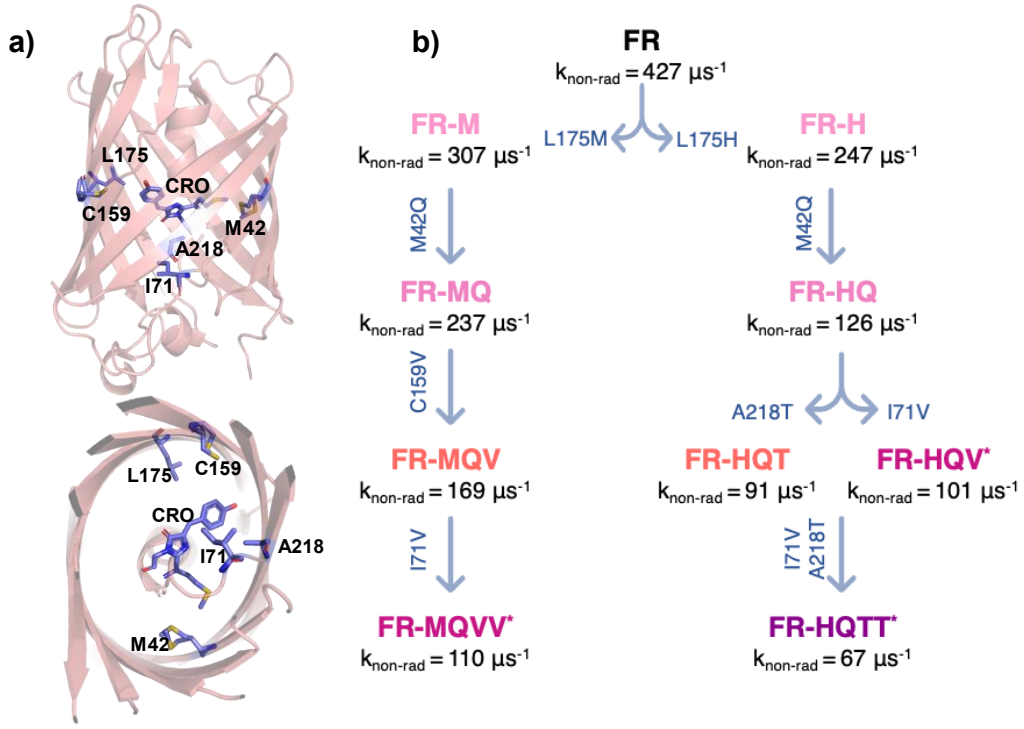

Figure 1. a) Crystal structure of FusionRed (PDB ID: 6U1A) shown in top and side views, highlighting relevant mutations. The numbering corresponds to the convention employed in our previous study, offset by one compared to the PDB structure. (b) An evolutionary tree illustrates the sequence of mutations and the decrease in the non-radiative rate constants along the series.

Our next target for saturation was H198, which is analogous to R197 in mCherry-XL and T203 in GFP variants. This residue is known to influence the electronic structure of the chromophore, resulting in distinct photophysical and spectral effects.[15,30] We performed saturation mutagenesis at H198 in FR, FR-HQ, and FR-MQV and confirmed H198 to be a conserved mutation with respect to fluorescence, consistent with our prior observations.[20] Next, we reconsider a pathway for extended fluorescence lifetime discovered in the

"FR-13" variant (FR: H23Y, V47I, F81Y and A218T).[29] In this case, the A218T mutation (designated as "FR-T") resulted in an increase in fluorescence lifetime, and quantum yield compared to FR. Examination of the crystal structure of FR suggests that A218 can interact with H198 (see Figure S2.5). However, when we performed saturation mutagenesis at H198 on the FR-A218T variant, we found that H198 was the sole fluorescent variant in this library. Interestingly, A218 is also situated within hydrogen bonding distances to residues in the turn-region of the α-helix of FR, most notably I71. Mutations at this position have been explored in the development of the latest generation of bright FPs, e.g. mScarlet-I and mScarlet3.[13] Based on these observations, we performed saturation mutagenesis at positions A218 and I71 on FR-MQV and FR-HQ to generate a library of 400 variants. Lifetime screening of this library revealed several variants with lifetimes exceeding 3.5 ns and quantum yields ≥ 65% (Supplementary Table S2.5). Within the FR-H lineage, including FR-HQ I71V (designated as "FR-HQV*"), FR-HQ A218T (designated as "FR-HQT"), and FR-HQ A218T I71T (designated as "FR-HQTT*") and within the lineage of FR-MQV mutants, we discovered FR-MQV I71V (designated as "FR-MQVV*"). The spectra and lifetime decays of these variants are provided in Figure 2.

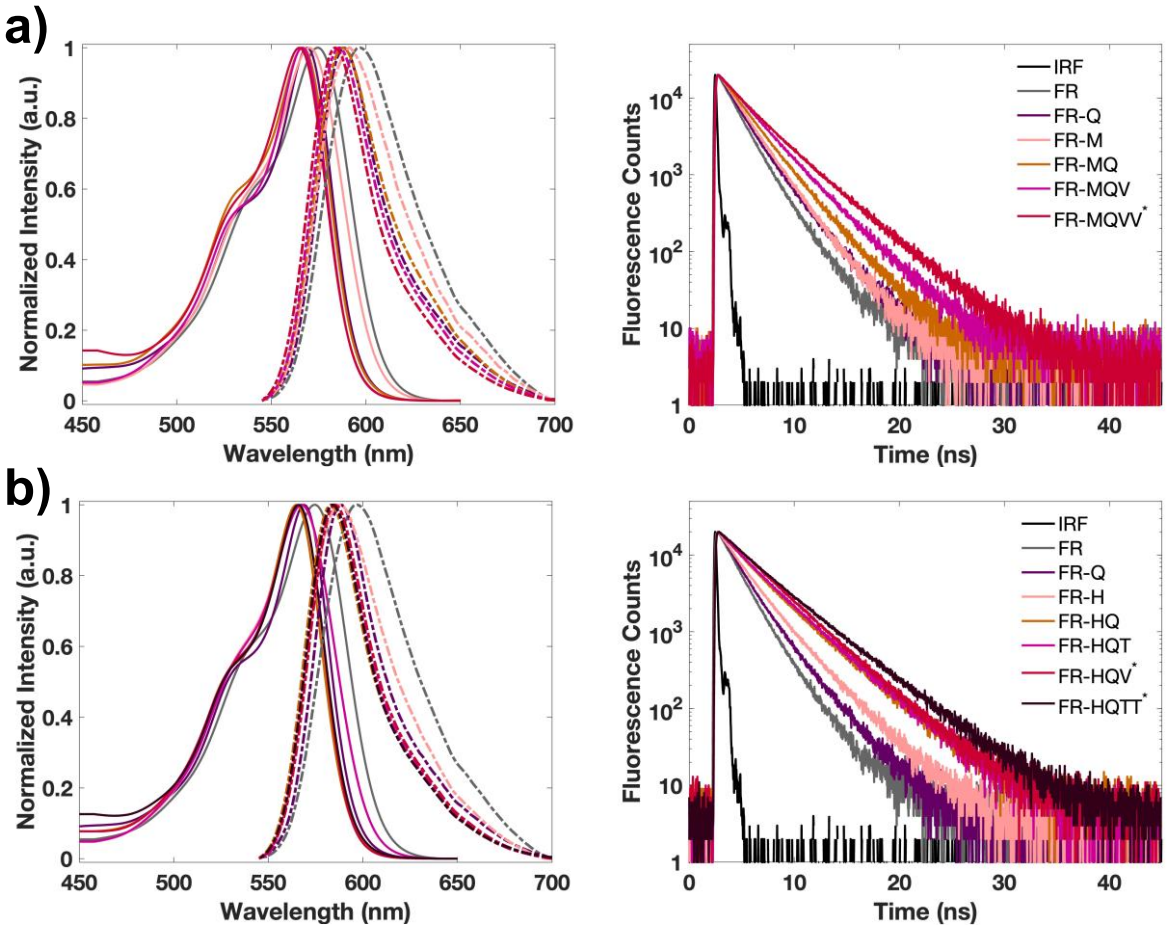

Figure 2. Steady state absorption (solid lines) and emission (dashed lines) spectra and fluorescence lifetime decays for a) FR-M lineage of proteins b) FR-H lineage of proteins. The spectra and lifetime traces follow the same color scheme as indicated in the legends for the lifetime decay traces.

MD simulations: We performed all-atom molecular dynamics simulations, spanning approximately 500 ns,[31] to evaluate the influence of single substitutions at positions 175, 42, 159, and 218 in FR. (SI Section S2b-e). Computational details are provided in Supplementary Information Section S1e. In the case of the

leucine to methionine substitution at position 175 (FR-M), the MD simulations showed a single sidechain conformer ~1.5 Å closer to the chromophore which supports the notion of a conformationally restricted environment near the phenol moiety (Figure S2.2b). Similarly, the FR-M42Q substitution (FR-Q) led to a 60% reduction in conformational variability on the acylimine end, as probed by the distance between the chromophore acylimine oxygen and the sidechain of Q42 (Figure S2.3b).

The trajectories also revealed that the conformational heterogeneity of C159 was influenced by its interaction with L175. The C159V substitution on FR resulted in reduced conformational heterogeneity and replicated the effect observed in the single FR L175M substitution, suggesting a significant impact of L175 on the chromophore interaction via C159. (Figure S2.4) The trajectories also suggest that the A218T mutation on FR introduced a strong hydrogen bond with residue H198 (d_{DA}~2 Å), implying that the conformational flexibility of the group at position 218 is correlated with the dynamics of critical residues such as H198 through a hydrogen-bonded network. (Figure S2.5) These results provide insights into the impact of specific amino acid substitutions on the chromophore and sidechain flexibility. The combination of these effects observed in MD trajectories of single mutants could be additive, resulting in long lifetimes and higher quantum yields, as observed in mutants such as FusionRed-MQVV*.

Table 2. Photophysical data for the FR variants and other RFPs discussed here. Please refer to Table 1 for sequences.

Protein	**$\lambda_{abs\ max}$ (nm)**	**$\lambda_{em\ max}$ (nm)**	**τ (ns)**	**ϕ (%)**	**ε_{max} ($M^{-1}cm^{-1}$)**	**B (ε_{max}*ϕ)**	**k_{rad} (μs^{-1})**	**$k_{non\text{-}rad}$ (μs^{-1})**
FR	574	596	1.78 ± 0.03	24 ± 2	94,000 ± 5,500	100	135	427
FR-Q	567	587	2.11± 0.03	34 ± 3	133,500 ± 7,500	200	161	311
FR-M	571	591	2.15 ± 0.01	34 ± 1	75,000 ± 6,500	113	158	307
FR-MQ	567	586	2.45± 0.03	43 ± 2	129,500 ± 5,500	246	175	237
FR-MQV	566	585	2.78 ± 0.06	53 (ref)	141,000 ± 9,500	330	191	169
FR-MQVV*	565	582	3.37 ± 0.01	64 ± 1	96,000 ± 6,500	273	196	110
FR-H	568	588	2.34 ± 0.04	42 ± 3	120,000 ± 4,000	223	178	247
FR-HQ	565	583	3.17 ± 0.10	60 ± 1	118,500 ± 10,500	316	189	126
FR-HQT	566	583	3.50 ± 0.01	68 ± 2	65,000 ± 15,000	196	194	91
FR-HQV*	566	585	3.36 ± 0.05	66 ± 3	123,500 ± 1,500	360	196	101
FR-HQTT*	566	583	3.74 ± 0.04	75 ± 4	65,500 ± 14,000	218	200	67
mCherry	587	609	1.67 ± 0.07	22 (Ref)	75,500 ± 5,000	75	137	488
mCherry XL	558	589	3.86 ± 0.05	70 ± 2	72,000 ± 4,000	223	179	76
mScarlet	569	592	3.87 ± 0.07	71 ± 2	104,000 ± 4,000	327	186	72

Photophysical characterization: Properties of the relevant FPs are detailed in Table 2, and spectra and fluorescence lifetime decays are shown in Figure 2 (additional fit details and characterization in Supplementary Information Section S3). The new FR variants display a linear scaling of fluorescence quantum yield with lifetime (Figure 3a). The slope indicates average radiative rate changes slightly versus non-radiative rate during lifetime evolution. Across the 20-75% fluorescence quantum yield range, the FR family's slope is about 1.25 times greater than mCherry variants, consistent with the higher extinction coefficients for FR-variants, compared to mCherry variants. Non-radiative rates consistently decrease with high quantum yield and lifetime, aligning with our mCherry findings and further supported by the works of Lin *et al*. and Drobizhev *et al*. utilizing electronic Stark and two-photon excitation spectroscopy to explore FP photophysics.[30, 32] Long-lifetime FR variants show minimal shifts (~5 nm) in peak wavelengths and ~10% changes in Stokes shifts (Figure 2). For example, the non-radiative rate constant for FR-HQV* is almost the half of its precursor FR-HQ, but their absorption and emission spectra are identical. This observation supports our previous analysis regarding mCherry variants, where the change in the energy gap does not appear to be the primary driver for reducing non-radiative rates.[15] Therefore, spectroscopic assessments to identify modes on the excited state manifold that can lead to ultrafast nonradiative pathways can be helpful to ascertain the drop in non-radiative rates.[33] Interestingly, M42Q near the chromophore's acylimine end yields significant spectral changes, (Stokes shift change of 75 cm^{-1} relative to FR) consistent with the findings of Moron *et al*. on the role of the acylimine dihedral angle in spectral shifts.[34] In the mCherry and mKate protein families, hydrogen-bonding interactions surrounding the acylimine end contribute to the far-red absorption and emission characteristics seen in FPs such as mPlum, mRojo, mNeptune, and TagRFP-675, albeit through different mechanisms.[35-39]

The maximum fluorescence quantum yield of 75% for FR-HQTT* is on par with those of the brightest RFPs such as mScarlet and mCherry-XL. Interestingly, in the latest generation of the mScarlet family, mScarlet3, the fluorescence quantum yield was only improved by 5%, with minimal spectral changes, despite significant advancements in chromophore maturation and cellular brightness.[13] This observation prompts a question about a potential theoretical limit for the MYG chromophore's fluorescence lifetime and quantum yield for a given absorption and emission spectra. Further exploration is needed to determine the origins of this apparent limit, whether it can be surpassed or is due to the interplay between chromophore electronic structure and its interactions with the environment. A Marcus-Hush-like analysis, analogous to the work of Lin et al., might unveil whether this trend is due to a theoretical "saturation point".[30]

Photostability and cellular brightness: This study focused on design of brighter FR variants by tuning conformational rigidity. However, from an applications perspective it is useful to assess the impact of the mutations on the properties of these FPs in cells. We measured photostability in bacteria and brightness in HeLa cells. We analyzed the photobleaching kinetics resulting from 561 nm widefield excitation normalized conditions at excitation rates of 600 s^{-1} and 1100 s^{-1} (corresponding to ~7.5 and 15 W/cm^2 for FR). These FPs exhibit both mono-exponential (FR V159 variants with mCherry-XL and mScarlet) and bi-exponential (FR C159 variants) decay kinetics, consistent with previous reports on FR variants (Figure S4.1). [20, 26] Previously, we discovered that the biexponential decay kinetics associated with C159 result from reversible photobleaching mechanisms.[20] Rather than solely relying on the traditional method of assessing photobleaching, which involves determining the half-life based on the 50% intensity value of fluorescence decay at a given irradiance, we opted to fit the photobleaching traces to exponentials. In doing so, we used the resulting half-life values obtained from either the mono-exponential trace or the longer component of the bi-exponential decay for these traces. (Methodology detailed in Supplementary

Information S4) This analysis allowed for a quantitative comparative analysis of permanent photobleaching within the family of FR variants generated in this study.[12]

Our analysis indicates that dark state conversion is a photoprotective mechanism for FPs with bi-exponential bleaching kinetics. FPs with similar or longer lifetimes than FR-MQV but which exhibit bi-exponential photobleaching kinetics had a lower quantum yield of photobleaching. At higher excitation rates, FPs such as FR-MQ, FR-HQ, and FR-HQV*, which have biexponential kinetics, show a reduction in the quantum yield of photobleaching (Figure 3b). This trend suggests that photostability is correlated with the propensity to convert to photoprotective (i.e., weakly absorbing) intermediate states. Investigations of the closely related FP TagRFP revealed that the nearly order of magnitude increase in photostability due to a S158T (equivalent to FR C159) mutation,[40,41] can be explained with a "circular restoration model" based on insights from a crystallographic study of TagRFP which revealed the presence of both cis and trans fluorescent forms. In this model, conversion between protonated (non-fluorescent) and deprotonated (fluorescent) forms of the chromophore's cis and trans-isomers comprise a photocycle which can "short-circuit" photobleaching in the S158T mutant, but not in TagRFP.[42] Recently, QM/MM simulations confirmed that mutations at C159 can limit chromophore "I-twist" motion in the excited electronic state.[43] Accordingly, the C159V mutation in FR may limit the chromophore conformation to a single cis form facing S144, away from V159, thus blocking access to the "circular restoration" photocycle. This proposal is consistent with our observation that the C159V mutation impairs reversible photoswitching in FR, where multi-exponential photobleaching kinetics at low irradiances (~1-10W/cm^2) are negligible (e.g., FR-MQVV*, mCherry, and mScarlet). These FPs may be more suitable for FRET-related applications where dark state conversion is undesirable. However, this behavior can change significantly at higher excitation rates which lead to shifts in the mechanisms of dark state conversion. Nevertheless, the significant observation here is that the creation of FPs with high molecular brightness is achievable without compromising the reversible photobleaching tendencies of the FP chromophore.

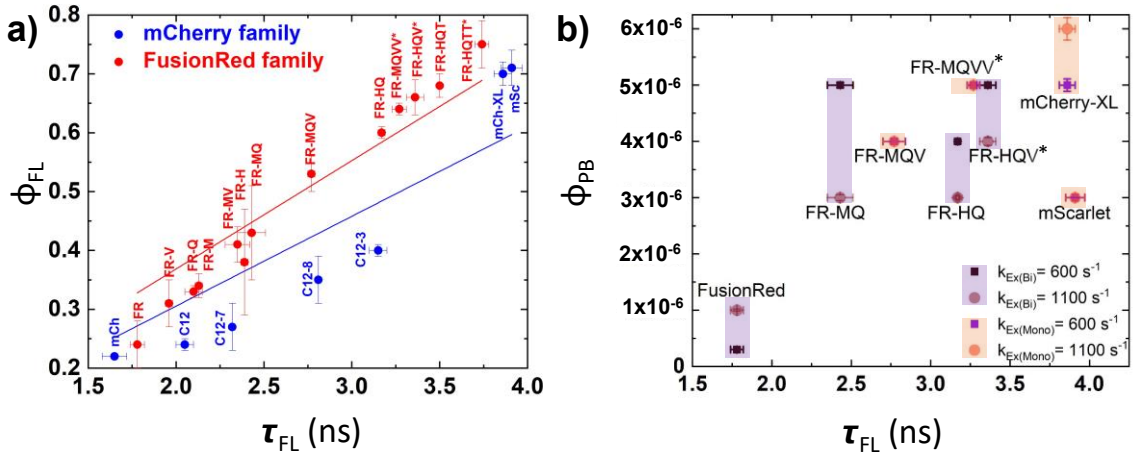

Figure 3. a) Fluorescence quantum yield (ϕ_{FL}) versus fluorescence lifetime (τ_{FL}): The slope of the linear relationship between fluorescence lifetime and fluorescence quantum yield reflects the average radiative rate constant. The higher slope (red) for FR mutants compared to mCherry mutants (and mScarlet; in blue) indicates a higher average radiative rate. b) The quantum yield of photobleaching (ϕ_{PB}) versus fluorescence lifetime (τ_{FL}): FPs with dark state conversion (highlighted in purple) exhibit a reduced quantum yield of photobleaching due to the possible presence of photoprotective dark states. The photobleaching quantum yield values for FR-MQV, FR-MQVV* and mScarlet are nearly the same at the two excitation rates.

Expression in HeLa cells and the subsequent assessment of brightness were conducted using piggyBac-H2B vectors and flow cytometry, as detailed in Supplementary Information Section S5. Our investigation aimed to quantify the cellular fluorescence brightness of three variants—FR-MQV, FR-MQVV*, and FR-HQV*—where chromophore maturation was not significantly diminished due to the incorporation of the A218T mutation. Human codon-optimized versions of the genes were purchased from a commercial gene synthesis company (Gene Universal, Newark Delaware, USA), who use a proprietary algorithm for optimization. The codon-optimized versions of FR-MQVV and FR-HQV exhibited a 1.3-fold increase in fluorescence brightness compared to the FR-MQV (mScarlet control). However, when compared to the non-codon optimized versions - we note a significant drop in the brightness of FR-MQV on codon optimization and this outcome is unexpected, as codon optimization traditionally enhances protein expression levels rather than diminishing them. Furthermore, the counterintuitive nature of this result becomes even more pronounced when considering the minimal divergence in codon composition between the variant and parent genes. This outcome underscores the complexity of predicting and interpreting the ramifications of codon optimization, particularly in cases where specific amino acid positions play a crucial role in protein structure and function. [44, 45]

Outlook: To develop variants of FR with longer fluorescence lifetimes and higher brightness, we performed targeted mutagenesis at positions previously shown to produce photophysical diversity, but which were not fully explored. In a series of library generations corroborated by MD simulations, we developed fluorophores with fluorescence quantum yields up to 75%. This study aids in the general advancement of fluorescent tool development and provides insights into identifying key positions, such as A218 in FR, that are useful for reducing the non-radiative rates by increasing the rigidity of the chromophore environment. The chances of discovering and understanding the significance of these mutations would have been limited when using high-throughput evolution tools with low information content, such as FACS. These ideas extend beyond experimental principles, with the emergence of AI-assisted in-silico methods such as AlphaFold and RosettaFold revolutionizing the design of synthetic proteins,[46,47] including FPs. Additionally, genetic code expansion, involving the incorporation of non-natural amino acids through engineered orthogonal translation systems in synthetic biology, presents a promising approach to creating a new generation of fluorescent tools driven by physical principles of reduced conformational space and ideal positioning indices for key residues around fluorescent chromophores.[48] Future efforts combining these methods could potentially generate new fluorophores surpassing the performance of the best currently available FPs.

ASSOCIATED CONTENT

Supporting Information: Supplementary Information (Sections S1 to S5) have been provided.

AUTHOR INFORMATION

Corresponding Author
Ralph Jimenez: rjimenez@jila.colorado.edu

Author Contributions

S.M., and R.J. conceptualized the study. S.M., and N.D. designed and performed the experiments. R.J. and S.M. designed and analyzed the simulations. S.M. and R.J. developed data analysis methods in the study. S.M., N.D., and R.J. wrote the manuscript.

Funding Sources

NSF Physics Frontier Center at JILA (PHY 2317149 to R.J.)

Notes

The authors declare no competing financial interest.

ACKNOWLEDGMENTS

S.M. was supported by the NIH/CU Molecular Biophysics Training Program (T32). This work was partially supported by the NSF Physics Frontier Center at JILA (PHY 2317149 to R.J.). R.J. is a member of the Quantum Physics Division of the National Institute of Standards and Technology (NIST). Certain commercial equipment, instruments, or materials are identified in this paper in order to specify the experimental procedure adequately. Such identification is not intended to imply recommendation or endorsement by the NIST, nor is it intended to imply that the materials or equipment identified are necessarily the best available for the purpose. Spectroscopy was performed at the W.M. Keck Optical Measurements Laboratory in JILA. We acknowledge Theresa Nahreini and the Flow Cytometry shared core facility at BioFrontiers Institute, CU Boulder (supported by NIH S10ODO21601). Finally, we also thank Prof. Amy E. Palmer, Prof. Prem P. Chapagain, Prof. ShengTing Hung, Dr. Premashis Manna and Jacob Kirsh for valuable discussions.

REFERENCES

1. Tsien, R. Y. The Green Fluorescent Protein. *Annu. Rev. Biochem.* **1998**, *67* (1), 509–544. https://doi.org/10.1146/annurev.biochem.67.1.509.

2. Shaner, N. C.; Steinbach, P. A.; Tsien, R. Y. A Guide to Choosing Fluorescent Proteins. *Nat. Methods* **2005**, *2* (12), 905–909. https://doi.org/10.1038/nmeth819.

3. Lambert, T. J. FPbase: A Community-Editable Fluorescent Protein Database. *Nature Methods.* **2019**, pp 277–278. https://doi.org/10.1038/s41592-019-0352-8.

4. Ai, H. W.; Baird, M. A.; Shen, Y.; Davidson, M. W.; Campbell, R. E. Engineering and Characterizing Monomeric Fluorescent Proteins for Live-Cell Imaging Applications. *Nat. Protoc.* **201**4, *9* (4), 910–928. https://doi.org/10.1038/nprot.2014.054.

5. Truong, L.; Ferré-D'Amaré, A. R. From Fluorescent Proteins to Fluorogenic RNAs: Tools for Imaging Cellular Macromolecules. *Protein Sci.* **2019**, *28* (8), 1374–1386. https://doi.org/10.1002/pro.3632.

6. Campbell, B. C.; Paez-Segala, M. G.; Looger, L. L.; Petsko, G. A.; Liu, C. F. Chemically Stable Fluorescent Proteins for Advanced Microscopy. *Nat. Methods* **2022**, *19* (12), 1612–1621. https://doi.org/10.1038/s41592-022-01660-7.

7. Bindels, D. S.; Haarbosch, L.; Van Weeren, L.; Postma, M.; Wiese, K. E.; Mastop, M.; Aumonier, S.; Gotthard, G.; Royant, A.; Hink, M. A.; Gadella, T. W. J. MScarlet: A Bright Monomeric Red Fluorescent Protein for Cellular Imaging. *Nat. Methods* **2016**, *14* (1), 53–56. https://doi.org/10.1038/nmeth.4074.

8. Legault, S.; Fraser-Halberg, D. P.; McAnelly, R. L.; Eason, M. G.; Thompson, M. C.; Chica, R. A. Generation of Bright Monomeric Red Fluorescent Proteins via Computational Design of Enhanced Chromophore Packing. *Chem. Sci.* **2022**. https://doi.org/10.1039/d1sc05088e.

9. Lambert, G. G.; Depernet, H.; Gotthard, G.; Schultz, D. T.; Navizet, I.; Lambert, T.; Adams, S. R.; Torreblanca-Zanca, A.; Chu, M.; Bindels, D. S.; Levesque, V.; Moffatt, J. N.; Salih, A.; Royant, A.; Shaner, N. C. Aequorea's Secrets Revealed: New Fluorescent Proteins with Unique Properties for Bioimaging and Biosensing. *PLoS Biol.* **2020**, *18* (11). https://doi.org/10.1371/journal.pbio.3000936.

10. Campbell, B. C.; Nabel, E. M.; Murdock, M. H.; Lao-Peregrin, C.; Tsoulfas, P.; Blackmore, M. G.; Lee, F. S.; Liston, C.; Morishita, H.; Petsko, G. A. mGreenLantern: A Bright Monomeric Fluorescent Protein with Rapid Expression and Cell Filling Properties for Neuronal Imaging. *Proc. Natl. Acad. Sci. U. S. A.* **2020**, *117* (48), 30710–30721. https://doi.org/10.1073/pnas.2000942117.

11. Hirano, M.; Ando, R.; Shimozono, S.; Sugiyama, M.; Takeda, N.; Kurokawa, H.; Deguchi, R.; Endo, K.; Haga, K.; Takai-Todaka, R.; Inaura, S.; Matsumura, Y.; Hama, H.; Okada, Y.; Fujiwara, T.; Morimoto, T.; Katayama, K.; Miyawaki, A. A Highly Photostable and Bright Green Fluorescent Protein. *Nat. Biotechnol.* **2022**, *40* (7), 1132–1142. https://doi.org/10.1038/s41587-022-01278-2.

12. Mukherjee, S.; Jimenez, R. Photophysical Engineering of Fluorescent Proteins: Accomplishments and Challenges of Physical Chemistry Strategies. *J. Phys. Chem. B* **2022**, *126* (4), 735–750. https://doi.org/10.1021/acs.jpcb.1c05629.

13. Gadella, T. W. J.; van Weeren, L.; Stouthamer, J.; Hink, M. A.; Wolters, A. H. G.; Giepmans, B. N. G.; Aumonier, S.; Dupuy, J.; Royant, A. mScarlet3: A Brilliant and Fast-Maturing Red Fluorescent Protein. *Nat. Methods* **2023**, *20* (4), 541–545. https://doi.org/10.1038/s41592-023-01809-y.

14. Goedhart, J.; Von Stetten, D.; Noirclerc-Savoye, M.; Lelimousin, M.; Joosen, L.; Hink, M. A.; Van Weeren, L.; Gadella, T. W. J.; Royant, A. Structure-Guided Evolution of Cyan Fluorescent Proteins towards a Quantum Yield of 93%. *Nat. Commun.* **2012**, *3*. https://doi.org/10.1038/ncomms1738.

15. Mukherjee, S.; Manna, P.; Hung, S. T.; Vietmeyer, F.; Friis, P.; Palmer, A. E.; Jimenez, R. Directed Evolution of a Bright Variant of MCherry: Suppression of Nonradiative Decay by Fluorescence Lifetime Selections. *J. Phys. Chem. B* **2022**, *126* (25), 4659–4668. https://doi.org/10.1021/acs.jpcb.2c01956.

16. Dean, K. M.; Lubbeck, J. L.; Davis, L. M.; Regmi, C. K.; Chapagain, P. P.; Gerstman, B. S.; Jimenez, R.; Palmer, A. E. Microfluidics-Based Selection of Red-Fluorescent Proteins with Decreased Rates of Photobleaching. *Integr. Biol. (United Kingdom)* **2015**, *7* (2), 263–273. https://doi.org/10.1039/c4ib00251b.

17. Dean, K. M.; Davis, L. M.; Lubbeck, J. L.; Manna, P.; Friis, P.; Palmer, A. E.; Jimenez, R. High-Speed Multiparameter Photophysical Analyses of Fluorophore Libraries. *Anal. Chem.* **2015**, *87* (10), 5026–5030. https://doi.org/10.1021/acs.analchem.5b00607.

18. Hung, S. T.; Mukherjee, S.; Jimenez, R. Enrichment of Rare Events Using a Multi-Parameter High Throughput Microfluidic Droplet Sorter. *Lab Chip* **2020**, *20* (4), 834–843. https://doi.org/10.1039/c9lc00790c.

19. Bindels, D. S.; Postma, M.; Haarbosch, L.; van Weeren, L.; Gadella, T. W. J. Multiparameter Screening Method for Developing Optimized Red-Fluorescent Proteins. Nat. Protoc. **2020**, 15 (2), 450–478. https://doi.org/10.1038/s41596-019-0250-7.

20. Mukherjee, S.; Hung, S. T.; Douglas, N.; Manna, P.; Thomas, C.; Ekrem, A.; Palmer, A. E.; Jimenez, R. Engineering of a Brighter Variant of the FusionRed Fluorescent Protein Using Lifetime Flow Cytometry and Structure-Guided Mutations. *Biochemistry* **2020**, *59* (39), 3669–3682. https://doi.org/10.1021/acs.biochem.0c00484.

21. Shemiakina, I. I.; Ermakova, G. V.; Cranfill, P. J.; Baird, M. A.; Evans, R. A.; Souslova, E. A.; Staroverov, D. B.; Gorokhovatsky, A. Y.; Putintseva, E. V.; Gorodnicheva, T. V.; Chepurnykh, T. V.; Strukova, L.; Lukyanov, S.; Zaraisky, A. G.; Davidson, M. W.; Chudakov, D. M.; Shcherbo, D. A Monomeric Red Fluorescent Protein with Low Cytotoxicity. *Nat. Commun.* **2012**, *3*, 1204. https://doi.org/10.1038/ncomms2208.

22. Yoon, S.; Pan, Y.; Shung, K.; Wang, Y. FRET-Based $Ca2^{+}$ Biosensor Single Cell Imaging Interrogated by High-Frequency Ultrasound. Sensors (Switzerland) **2020**, 20 (17), 1–14. https://doi.org/10.3390/s20174998.

23. Chernov, K. G.; Manoilov, K. Y.; Oliinyk, O. S.; Shcherbakova, D. M.; Verkhusha, V. V. Photodegradable by Yellow Orange Light DegFusionRed Optogenetic Module with Autocatalytically Formed Chromophore. Int. J. Mol. Sci. **2023**, 24 (7). https://doi.org/10.3390/ijms24076526.

24. Muslinkina, L.; Pletnev, V. Z.; Pletneva, N. V.; Ruchkin, D. A.; Kolesov, D. V.; Bogdanov, A. M.; Kost, L. A.; Rakitina, T. V.; Agapova, Y. K.; Shemyakina, I. I.; Chudakov, D. M.; Pletnev, S. Two Independent Routes of Post-Translational Chemistry in Fluorescent Protein FusionRed. *Int. J. Biol. Macromol.* **2020**, *155*, 551–559. https://doi.org/10.1016/j.ijbiomac.2020.03.244.

25. Pennacchietti, F.; Serebrovskaya, E. O.; Faro, A. R.; Shemyakina, I. I.; Bozhanova, N. G.; Kotlobay, A. A.; Gurskaya, N. G.; Bodén, A.; Dreier, J.; Chudakov, D. M.; Lukyanov, K. A.; Verkhusha, V. V.; Mishin, A. S.; Testa, I. Fast Reversibly Photoswitching Red Fluorescent Proteins for Live-Cell RESOLFT Nanoscopy. *Nat. Methods* **2018**, *15* (8), 601–604. https://doi.org/10.1038/s41592-018-0052-9.

26. Mukherjee, S.; Thomas, C.; Wilson, R.; Simmerman, E.; Hung, S. T.; Jimenez, R. Characterizing Dark State Kinetics and Single Molecule Fluorescence of FusionRed and FusionRed-MQ at Low Irradiances. *Phys. Chem. Chem. Phys.* **2022**, *24* (23), 14310–14323. https://doi.org/10.1039/d2cp00889k.

27. Klementieva, N. V.; Pavlikov, A. I.; Moiseev, A. A.; Bozhanova, N. G.; Mishina, N. M.; Lukyanov, S. A.; Zagaynova, E. V.; Lukyanov, K. A.; Mishin, A. S. Intrinsic Blinking of Red Fluorescent Proteins for Super-Resolution Microscopy. *Chem. Commun.* **2017**, 53 (5), 949–951. https://doi.org/10.1039/c6cc09200d.

28. Yoon, E.; Konold, P. E.; Lee, J.; Joo, T.; Jimenez, R. Far-Red Emission of MPlum Fluorescent Protein Results from Excited-State Interconversion between Chromophore Hydrogen-Bonding States. *J. Phys. Chem. Lett.* **2016**, *7* (12), 2170–2174. https://doi.org/10.1021/acs.jpclett.6b00823.

29. Manna, P.; Hung, S. T.; Mukherjee, S.; Friis, P.; Simpson, D. M.; Lo, M. N.; Palmer, A. E.; Jimenez, R. Directed Evolution of Excited State Lifetime and Brightness in FusionRed Using a Microfluidic Sorter. *Integr. Biol. (United Kingdom)* **2018**, *10* (9), 516–526. https://doi.org/10.1039/c8ib00103k.

30. Lin, C. Y.; Romei, M. G.; Oltrogge, L. M.; Mathews, I. I.; Boxer, S. G. Unified Model for Photophysical and Electro-Optical Properties of Green Fluorescent Proteins. *J. Am. Chem. Soc.* **2019**, *141* (38), 15250–15265. https://doi.org/10.1021/jacs.9b07152.

31. Mukherjee, S.; Manna, P.; Douglas, N.; Chapagain, P. P.; Jimenez, R. Conformational Dynamics of mCherry Variants: A Link between Side-Chain Motions and Fluorescence Brightness. *J. Phys. Chem. B* **2023**, *127* (1), 52–61. https://doi.org/10.1021/acs.jpcb.2c05584.

32. Drobizhev, M.; Molina, R. S.; Callis, P. R.; Scott, J. N.; Lambert, G. G.; Salih, A.; Shaner, N. C.; Hughes, T. E. Local Electric Field Controls Fluorescence Quantum Yield of Red and Far-Red Fluorescent Proteins. *Front. Mol. Biosci.* **2021**, *8* (February), 1–21. https://doi.org/10.3389/fmolb.2021.633217.

33. Chen, C.; Henderson, J. N.; Ruchkin, D. A.; Kirsh, J. M.; Baranov, M. S.; Bogdanov, A. M.; Mills, J. H.; Boxer, S. G.; Fang, C. Structural Characterization of Fluorescent Proteins Using Tunable Femtosecond Stimulated Raman Spectroscopy. *International Journal of Molecular Sciences*. **2023**. https://doi.org/10.3390/ijms241511991.

34 . Moron, V.; Marazzi, M.; Wanko, M. Far Red Fluorescent Proteins: Where Is the Limit of the Acylimine Chromophore? *J. Chem. Theory Comput.* **2019**, *15* (7), 4228–4240. https://doi.org/10.1021/acs.jctc.9b00070.

35. Abbyad, P.; Childs, W.; Shi, X.; Boxer, S. G. Dynamic Stokes Shift in Green Fluorescent Protein Variants. *Proc. Natl. Acad. Sci. U. S. A.* **2007**, *104* (51), 20189–20194. https://doi.org/10.1073/pnas.0706185104.

36.Konold, P.; Regmi, C. K.; Chapagain, P. P.; Gerstman, B. S.; Jimenez, R. Hydrogen Bond Flexibility Correlates with Stokes Shift in mPlum Variants. *J. Phys. Chem. B* **2014**, *118* (11), 2940–2948. https://doi.org/10.1021/jp412371y.

37. Faraji, S.; Krylov, A. I. On the Nature of an Extended Stokes Shift in the mPlum Fluorescent Protein. *J. Phys. Chem. B* **2015**, *119* (41), 13052–13062. https://doi.org/10.1021/acs.jpcb.5b07724.

38. Yoon, E.; Konold, P. E.; Lee, J.; Joo, T.; Jimenez, R. Far-Red Emission of mPlum Fluorescent Protein Results from Excited-State Interconversion between Chromophore Hydrogen-Bonding States. *J. Phys. Chem. Lett.* **2016**, *7* (12), 2170–2174. https://doi.org/10.1021/acs.jpclett.6b00823.

39. Chica, R. A.; Moore, M. M.; Allen, B. D.; Mayo, S. L. Generation of Longer Emission Wavelength Red Fluorescent Proteins Using Computationally Designed Libraries. Proc. Natl. Acad. Sci. U. S. A. **2010**,107 (47), 20257–20262. https://doi.org/10.1073/pnas.1013910107.

40. Shaner, N. C.; Lin, M. Z.; McKeown, M. R.; Steinbach, P. A.; Hazelwood, K. L.; Davidson, M. W.; Tsien, R. Y.Improving the Photostability of Bright Monomeric Orange and Red Fluorescent Proteins. *Nat. Methods* **2008**, *5* (6), 545–551. https://doi.org/10.1038/nmeth.1209.

41. Dean, K. M.; Lubbeck, J. L.; Binder, J. K.; Schwall, L. R.; Jimenez, R.; Palmer, A. E. Analysis of Red-Fluorescent Proteins Provides Insight into Dark-State Conversion and Photodegradation. *Biophys. J.* **2011**, *101* (4), 961–969. https://doi.org/10.1016/j.bpj.2011.06.055.

42. Liu, R.; Liang, Q. N.; Du, S. Q.; Hu, X. J.; Ding, Y. The Crystal Structure of Red Fluorescent Protein TagRFP-T Reveals the Mechanism of Its Superior Photostability. *Biochem. Biophys. Res. Commun.* **2016**, *477* (2), 229–234. https://doi.org/10.1016/j.bbrc.2016.06.047.

43. Murphy, A. R.; Hix, M. A.; Walker, A. Exploring the Effects of Mutagenesis on FusionRed Using Excited State QM/MM Dynamics and Classical Force Field Simulations. ChemBioChem **2023**, 24 (12), e202200799. https://doi.org/10.1002/cbic.202200799.

44. Ranaghan, M. J.; Li, J. J.; Laprise, D. M.; Garvie, C. W. Assessing Optimal: Inequalities in Codon Optimization Algorithms. *BMC Biol.* **2021**, *19* (1), 36. https://doi.org/10.1186/s12915-021-00968-8.

45. Mauro, V. P.; Chappell, S. A. A Critical Analysis of Codon Optimization in Human Therapeutics. *Trends Mol. Med.* **2014**, *20* (11), 604–613. https://doi.org/10.1016/j.molmed.2014.09.003.

46. Jumper, J.; Evans, R.; Pritzel, A.; Green, T.; Figurnov, M.; Ronneberger, O.; Tunyasuvunakool, K.; Bates, R.; Žídek, A.; Potapenko, A.; Bridgland, A.; Meyer, C.; Kohl, S. A. A.; Ballard, A. J.; Cowie, A.; Romera-Paredes, B.; Nikolov, S.; Jain, R.; Adler, J.; Back, T.; Petersen, S.; Reiman, D.; Clancy, E.; Zielinski, M.; Steinegger, M.; Pacholska, M.; Berghammer, T.; Bodenstein, S.; Silver, D.; Vinyals, O.; Senior, A. W.; Kavukcuoglu, K.; Kohli, P.; Hassabis, D. Highly Accurate Protein Structure Prediction with AlphaFold. *Nature* **2021**, 596 (7873), 583–589. https://doi.org/10.1038/s41586-021-03819-2.

47. Baek, M.; DiMaio, F.; Anishchenko, I.; Dauparas, J.; Ovchinnikov, S.; Lee, G. R.; Wang, J.; Cong, Q.; Kinch, L. N.; Dustin Schaeffer, R.; Millán, C.; Park, H.; Adams, C.; Glassman, C. R.; DeGiovanni, A.; Pereira, J. H.; Rodrigues, A. V.; Van Dijk, A. A.; Ebrecht, A. C.; Opperman, D. J.; Sagmeister, T.; Buhlheller, C.; Pavkov-Keller, T.; Rathinaswamy, M. K.; Dalwadi, U.; Yip, C. K.; Burke, J. E.; Christopher Garcia, K.; Grishin, N. V.; Adams, P. D.; Read, R. J.; Baker, D. Accurate Prediction of Protein Structures and Interactions Using a Three-Track Neural Network. *Science* (80-.). **2021**, 373 (6557), 871–876. https://doi.org/10.1126/science.abj8754.

48. Link, A. J.; Mock, M. L.; Tirrell, D. A. Non-Canonical Amino Acids in Protein Engineering. Curr. Opin. Biotechnol. **2003**, 14 (6), 603–609. https://doi.org/10.1016/j.copbio.2003.10.011.